

# PERFORMANCE COMPARISON OF A SIX PHASE SURFACE-MOUNDED PMSM WITH INNER AND OUTER ROTOR TYPES FOR HIGH TORQUE APPLICATIONS

Vuong Dang QUOC<sup>1,2</sup> , Trinh Cong TRUONG<sup>2</sup> , Thanh Nguyen VU<sup>1,2</sup> , Ha Vo THANH<sup>3</sup> 

<sup>1</sup>Laboratory of High performance electric machines (HiPems)

<sup>2</sup>School of Electrical and Electronic Engineering, Hanoi University of Science and Technology, No.1, Dai Co Viet Street, Hai Ba Trung District, Hanoi, Viet Nam

<sup>3</sup>Department of Cybernetics, Faculty of Electrical and Electronic Engineering, University of Transport and Communications, Ha Noi, Viet Nam

vuong.dangquoc@hust.edu.vn, trinh.truongcong@hust.edu.vn, thanh.nguyenvu@hust.edu.vn, vothanhhha.ktd@utc.edu.vn

DOI: 10.15598/aeee.v22i2.5536

Article history: Received Nov 05, 2023; Revised Apr 10, 2023; Accepted Apr 15, 2024; Published Jun 30, 2024. This is an open access article under the BY-CC license.

**Abstract.** Permanent magnet synchronous motors (PMSMs) have been widely applied in the fields of electric cars/strucks and industries due to their high torque and efficiency, reliable performance, simple structure and various shapes and sizes. Recently, multi-phase PMSMs with inner and outer configurations have been applied to the above applications. However, the investigation, evaluation and comparison performances of multi-phase PMSM with inner and outer rotor types in previous studies have not been fully presented in both the analytical model and finite element technique. The previous researches mainly have focussed on doing experiments without presenting the detail of design of these machines. In this context, electromagnetic parameters (such as electromagnetic torque, cogging torque, torque ripple, back electromagnetic force, linkage flux) of a six-phase surface mounted PMSM (SPMSM) with inner and outer rotor configurations is proposed via an association of analytic model and finite element method (FEM). The development of the proposed methods is focussed on a 145kW six-phase SPMSM with two distinct rotor structures (inner and outer rotors)

*tive force (EMF), cogging torque, torque ripple, analytical model, finite element method.*

## 1. Introduction

Recently, many researchers, designers, and manufacturers, both locally and abroad, have been no longer unfamiliar with permanent magnet synchronous motors (PMSMs). These motors are reliable, durable, safe, and offer a wide speed range, high torque, power density, and high efficiency [1–10]. Due to the position of rotor, the PMSM can be classified into inner rotor (IR) and outer rotor (OR) types. With the same volume, the OR technology can provides more physical space when compared to the IR topology [21], [22]. As a result, their wide range of applications are highly valued in the aerospace, medical, industrial, and military sectors. They are specifically utilized in applications such as electrical drive systems for drones, electric traction devices, collaborative robotics, and electric cars. Thus, numerous studies focusing on three-phase PMSMs have been published so far. In applications that require high dependability, six-phase PMSMs have been proposed as a way to improve the fault tolerance and reliability of three-phase PMSMs. Thus so far, certain researchers have also examined these kinds of motors. In reference [1], a novel electric vehicle application utilizing a stator-shifted six-phase

## Keywords

*Six-phase surface-mounted permanent magnet synchronous motor (SPMSM), back electromo-*

fractional-slot concentrated winding ferrite spoke-type PMSM was presented. This machine design consists of a rotor with ferrite permanent magnets (PMs) organized in a spoke pattern and a stator with two three-phase windings set 75 degrees apart. In reference [2], an innovative toroidal winding (NTW) design in a novel six-phase double-delta (PMSM) was provided to study the losses, back-EMF, cogging torque, total torque, and distribution of the magnetic field. Every NTW coil in this study is wound consistently and in the same direction onto the stator yoke. The obtained results showed that the suggested six-phase DDPMSM with NTWs offers highly desirable features for direct-drive systems, such as improved low-speed performance and increased torque output, in contrast to the conventional six-phase PMSM. A five-phase external rotor permanent magnet assisted synchronous reluctance motor (PMSynRM) with two different winding configurations was tested for performance in reference [3]. Compared to traditional three-phase winding, the use of a five-phase winding architecture offered improvements in power density, fault tolerance, and torque pulsation mitigation in the context of vehicle applications. Furthermore, using an external rotor architecture helps to achieve even higher power densities. In reference [4], the study presented a design methodology specifically designed for pulse-width modulation voltage source inverter (PWM VSI)-powered multi-phase PMSMs. First, the possibility of improving torque density by means of harmonic usage is introduced. Next, the unique difficulties arising from the multi-phase machines' PWM power supply throughout the design phase are discussed. In reference [5], a new winding configuration with eight poles and eight slots for six-phase PM machines was developed with the aim of reducing or eliminating unwanted space harmonics in the stator magnetomotive force (MMF). This study suggested designing a six-phase PM machine as two independent three-phase windings in order to increase drive train availability for use in electric vehicles (EVs). A novel configuration for a six-phase direct-drive PMSM with the  $60^\circ$  phase-belt toroidal winding configuration ( $60^\circ$ -TW) was presented in reference [6]. In this study, the finite element method (FEM) was used to compute the torque output, losses, back-electromotive force (EMF), and distribution of the magnetic field. In contrast to traditional winding techniques that involve coils that overlap, the  $60^\circ$ -TW's coils were all wound on the stator yoke in the same direction. The modeling and analysis of a six-phase SPMSM with an inner rotor (IR) based on an analogous magnetic network was reported in reference [7]. This research required an understanding of the electrical and magnetic characteristics of the machine as well as their interactions. In reference [8], using the dq-axis theory, a mathematical model for the six-phase interior permanent magnet synchronous motor (IPMSM) was created. This model was then applied to determine

the exact correlations between various per-unitized machine parameters in order to attain the best possible performance in both traction and inverter control (IC) scenarios. In reference [9], an equivalent magnetic network (EMN) model was presented for assessing the machine performance under demagnetization, using a six-phase surface-mounted PMSM as an example. The variable coercivity of PM was introduced to realize the rapidly building EMN models under various types of demagnetization. Comparisons were made between the air-gap flux density and the no-load back EMF determined by the FEM, the suggested EMN model, and the experimental testing. The findings shown that the six-phase surface-mounted PMSM under various demagnetization types may be accurately and quickly modelled using the suggested EMN model. In reference [10], the design, development, and testing of an advanced IPMSM that was created to satisfy the requirements of the FreedomCar 2020 specifications. The segmented stator construction of the 12 slot/10 pole machine is outfitted with FSCWs. The spoke construction of the rotor is unique. A number of prototypes featuring various heat control strategies have been constructed and evaluated. The test results for each of these prototypes will be discussed, along with the tradeoffs between the different approaches. In other words [21], [22], the papers demonstrated outer rotor (OR) PMSMs have larger torque density, or torque per rotor volume, when compared to inner rotor PMSMs. However, the copper loss occurs in armature winding, which generates the heat. Thus in terms of heat dissipation, the IR type with outside stator can be refrigerated easier than the OR configuration.

As previously mentioned, a great deal of research has been done on six-phase PMSMs. Nonetheless, there are still a lot of gaps in the amount of studies on this kind of motor. In particular, while studying this kind of motor, writers have mostly given the specifications of six-phase PMSMs and then carried out experiments on these devices without offering comprehensive formulas for calculating and analyzing the electromagnetic properties of these PMSMs. In particular, the evaluation and comparison performances of six-phase PMSM with IR and OR types have not been fully designed in both the analytical model and FEM.

In this context, electromagnetic parameters (such as electromagnetic torque, cogging torque, torque ripple, back electromagnetic force, linkage flux) of a six-phase surface mounted PMSM (SPMSM) with inner and outer rotor configurations is proposed via an association of analytic model and finite element method (FEM). The development of the proposed methods is focussed on a 145kW six-phase SPMSM with two distinct rotor structures (IR and OR configurations).

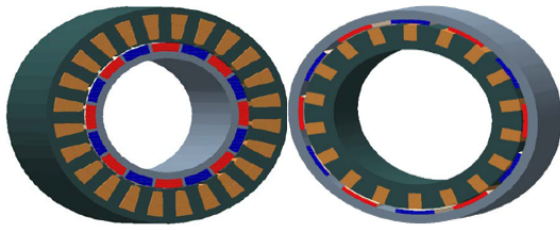


Fig. 1: Modeling of PMSM with IR and OR types [13].

Tab. 1: Main parameters of the SPMSM with OR.

| Parameters           | Value | Unit      |
|----------------------|-------|-----------|
| Rated power          | 145   | kW        |
| DC Bus Voltage       | 600   | V         |
| Number of phases     | 6     | phase     |
| Number of slots      | 24    | Slot      |
| Number of pole pairs | 4     | pole pair |
| Rated torque         | 1055  | Nm        |

## 2. Analytical design of PMSM with IR and OR types

The modelling of PMSM with IR and OR configurations is presented in Fig. 1 [13]. There are two different rotor structure (IR and OR) types are proposed for this investigation. In the design process, the PM creates the magnetic field in the air gap, determining the parameters for the PM is a crucial step in the design process. The width, thickness, length, and coverage angle (sometimes referred to as the pole embrace) of the PM in the PMSM are all determined by the strength of this field.

Fig. 2 illustrates the polarization (J) and magnetic flux density (B) as a function of demagnetizing field (H) for the NdFeB N38SH magnet utilized in this investigation. At 20°C, the magnet’s remanence is 1.26T, and its normal working point is 0.9T.

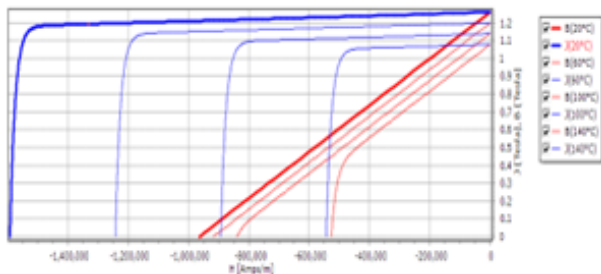


Fig. 2: Demagnetization curves for N38SH [19].

This section will presents a 145kW SPMSM with OR type, the obtained results on electromagnetic parameters are then compared with that of SPMSM with IR

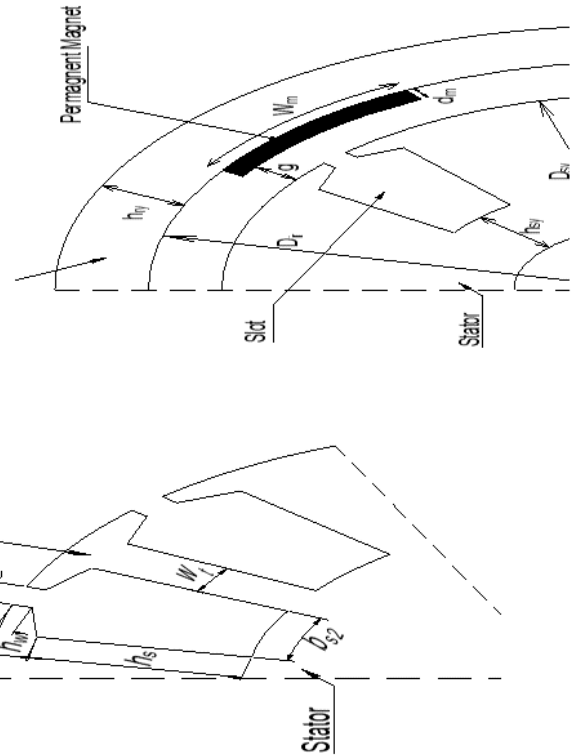


Fig. 3: Main dimensions of the magnetic core (top) and slot (bottom).

structure. Main parameters of the SPMSM with OR type are already given in Table 1. The main dimensions of the magnetic core and slot are modeled in Fig. 3.

The following formula can be used to get the fundamental flux density in the air gap [23]:

$$B_g = \frac{4}{\pi} \sin(\alpha) B_m, \tag{1}$$

where  $\alpha$  and  $B_m$  denote the PM typical operating flux density and the half coverage angle, both of which were expressed in electrical degrees. The thickness of the PM can be calculated as [23]:

$$d_m = \frac{\mu_m g_{eff}}{\frac{B_r \cdot 4 \sin(\alpha)}{B_g \pi} - 1}, \tag{2}$$

where  $\mu_m$ ,  $g_{eff}$  and  $B_r$  stand for the PM’s permeability, effective airgap length, and remanence, in that order. Note that the physical airgap length ( $g$ ), which is determined by the Carter’s factor, is not employed in this calculation [23]; instead, the  $g_{eff}$  is:

$$g_{eff} = k_c \cdot g, \tag{3}$$

where Carter’s factor  $k_c$  can be expressed as:

$$k_c = \frac{\tau_s}{\tau_s - \gamma g}, \tag{4}$$

where  $\tau_s$  is the slot pitch

$$\tau_s = \frac{\pi(D_{ir} - 2g)}{Z}, \quad (5)$$

where  $D_{ir}$  and  $Z$  stand for the rotor's inner diameter and slot count, respectively. The formula for determining the PM motor's factor ( $\gamma$ ) can be found in [23]:

$$\gamma = \frac{2b}{\pi g} \left[ \arctan \left( \frac{b_{so}}{2(L+g)} \right) - \frac{L+g}{b_{so}} \ln \sqrt{1 + \left( \frac{b_{so}}{2(L+g)} \right)^2} \right], \quad (6)$$

where  $L$  is the PM's length, which in this case is equal to the length of the rotor and stator, and  $b_{so}$  is the slot opening width. The width of PM ( $w_m$ ) is then defined:

$$w_m = \frac{\alpha D_{ir}}{p}, \quad (7)$$

where  $p$  is the number of pole pair.

As a crucial factor in figuring out the  $D_{ir}$  and the machine's length  $L$ , the armature part's volume can be computed as follows [23]:

$$\frac{\pi}{4} D_{ir}^2 L = \frac{M_n k_{safe}}{2\sigma_m}, \quad (8)$$

where  $M_n$  is the motor's rated torque,  $\sigma_m$  is the maximum shear stress that PM material can withstand ( $\sigma_m = 20 - 50\text{kPa}$ ), and  $k_{safe}$  is the safe factor ( $k_{safe} = 2 - 3$ ). It should be noted that the shaping coefficient, which is the ratio of the two parameters as indicated below, presents the relationship between the rotor's inner diameter and length, i.e.,

$$k_{shape} = \frac{L}{D_{ir}}. \quad (9)$$

From the equation (9) and (9), the value of  $D_{ir}$  and  $L$  can be computed.

The height of stator and rotor yokes ( $h_{sy}$ ) can be respectively determined as:

$$h_{sy} = \frac{B_m w_m}{2B_{sy}}, \quad (10a)$$

$$h_{ry} = \frac{B_m w_m}{2B_{ry}}, \quad (10b)$$

where the terms  $B_{sy}$  and  $B_{ry}$  are respectively the values of magnetic loading at the stator and rotor yokes. The width of tooth is:

$$w_t = \frac{2pB_m w_m}{B_t} \quad (11)$$

where  $Z$  and  $B_t$  are respectively the number of slot and values of magnetic loading at the tooth. These values can be found in [24].

The number of conductors per coil can be then defined as:

$$N_c = \frac{U_{phase}}{2\pi\sqrt{2}f q k_w B_g \cos \delta D_{ir} L}, \quad (12)$$

where  $k_w$ ,  $\delta$ ,  $q$ ,  $U_{phase}$  and  $f$  stand for the winding factor, torque angle, number of slots per pole per phase, phase voltage, and frequency, respectively. Typically, the PMSM torque angle is selected as 20 degrees [25]. The slot area can be calculated as:

$$A_{slot} = \frac{4N_c A_{Cu}}{k_{fill}}, \quad (13)$$

where  $A_{Cu}$ ,  $k_{fill}$  are the copper area of the conductor and the slot filling factor. The slot top width  $b_{s1}$ , slot bottom width  $b_{s2}$ , slot height  $h_s$  can be calculated as:

$$b_{s1} = \frac{\pi(D_{os} - 2h_{so} - 2h_w)}{Z} - \frac{2pB_m w_m}{Z B_t}, \quad (14)$$

$$b_{s2} = \sqrt{\frac{b_{s1}^2 - 4\pi \cdot A_{slot}}{Z}}, \quad (15)$$

$$h_s = \frac{2A_{slot}}{b_{s1} + b_{s2}}, \quad (16)$$

where  $h_{so}$ ,  $h_w$  are the height of the slot opening and the wedge respectively.

Based on the analytical theory developed above, a 145kW six-phase PMSM with IR and OR configurations is considered. The results on main dimensions of the proposed model are given in Table 2.

**Tab. 2:** Main dimensions of a six-phases PMSM of 145kW

| Parameters               | Inner Rotor | Outer Rotor | Unit    |
|--------------------------|-------------|-------------|---------|
| Stator outer diameter    | 430,4       | 308,8       | mm      |
| Stator inner diameter    | 323,7       | 165,3       | mm      |
| Rotor outer diameter     | 308,8       | 379,1       | mm      |
| Rotor inner diameter     | 250,2       | 323,7       | mm      |
| Iron core active length  | 323,7       | 323,7       | mm      |
| Stator yoke height       | 29,33       | 27,5        | mm      |
| Rotor yoke height        | 29,33       | 27,5        | mm      |
| Tooth width              | 15,2        | 15,32       | mm      |
| Slot depth               | 24          | 44,2        | mm      |
| Magnet thickness         | 5,5         | 5,5         | mm      |
| Magnet pole arc (EDeg)   | 130         | 130         | degrees |
| Air gap length           | 2           | 2           | mm      |
| Number of turns per coil | 6           | 7           | turns   |

### 3. Analysis of cogging torque

As we have known, the cogging torque that can cause noise and vibration in SPMSM with IR and OR types [15, 16]. When the SPMSM is used in variable speed drive applications, it can intensify the noise and vibration caused by the cogging torque if the frequency of torque fluctuations matches the stator or rotor's mechanical resonance frequency. Therefore, it is crucial to address and resolve this issue in order to design and produce high-performance PMSMs.

The following equations give the formula for computing the cogging torque ( $T_{cog}$ ) [17–20]:

$$T_{cog}(\theta) = \frac{2L_a B_\sigma^2 N_s p}{\pi \mu_0 N_L} (R_{in}^2 - R_{out}^2) T_k, \quad (17)$$

$$T_k = \sum_{k=1}^{\infty} \frac{K_{sk}}{k} \sin\left(k N_L \frac{b_0}{2}\right) \times \sin\left(k N_L \frac{\alpha_p}{2p}\right) \sin\left(k N_L \left(\theta - \frac{\alpha_s}{2p}\right)\right), \quad (18)$$

$$K_{sk} = \frac{2 \sin(K N_L \alpha_s / 2)}{k N_L \alpha_s}, \quad (19)$$

where  $L_a$  is the motor's effective axial length;  $B_\sigma$  is the maximum air-gap flux density brought about by the permanent magnets;  $N_s$  is the number of slots;  $N_L$  is the lowest common multiple of  $N_s$  and  $2p$ ;  $\mu_0$  is the air permeability;  $R_{in}$  and  $R_{out}$  are the inner and outer radii of the air gap;  $b_0$  is the slot opening;  $\alpha_p$  is the ratio of pole-arc to pole-pitch;  $\alpha_s$  is the skewing angle; and  $K_{sk}$  is the skew factor.

### 4. Finite element background

The theory and mathematical foundation for the entire PMSM analysis are already presented in Section III. In this part, Maxwell's Equation must be solved in order to analyze electromagnetic parameters to compare performances of the proposed SPMSM with IR and OR configurations. The equations for each of these terms, from (1) to (4), are written below [25, 26]:

$$\nabla \times \mathbf{H} = \mathbf{J}_s, \quad (20)$$

$$\nabla \times \mathbf{E} = -j\omega \mathbf{B}, \quad (21)$$

$$\nabla \cdot \mathbf{B} = 0, \quad (22)$$

where  $\mathbf{H}$  is the magnetic field (A/m),  $\mathbf{E}$  is the electric field (V/m),  $\mathbf{B}$  is the magnetic flux density (T), and  $\mathbf{J}_s$  is the current density (A/m<sup>2</sup>).

The above equations from (20) to (22) are solved with constitutive laws and boundary conditions (BCs), i.e., [26]:

$$\mathbf{B} = \mu \mathbf{H}, \quad (23a)$$

$$\mathbf{J} = \sigma \mathbf{E}, \quad (23b)$$

$$\mathbf{n} \times \mathbf{H}|_{\gamma_h} = 0, \quad (24a)$$

$$\mathbf{n} \cdot \mathbf{B}|_{\gamma_e} = 0, \quad (24b)$$

where  $\mu$  and  $\sigma$  stand for relative permeability and electric conductivity (S/m), respectively, and  $\mathbf{J}$  is the eddy current density (A/m<sup>2</sup>). The term  $\mathbf{B}$  in (21) is obtained from a vector potential  $\mathbf{A}$  such that

$$\mathbf{B} = \nabla \times \mathbf{A}. \quad (25)$$

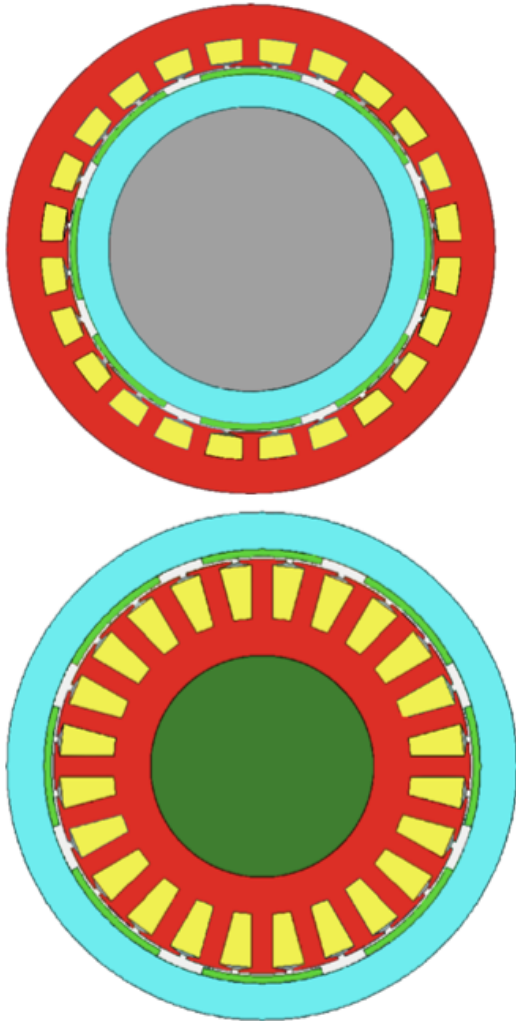


Fig. 4: 2D Geometry of the SPMSM with IR (top) and OR (bottom).

In general, the electromagnetic torque ( $T$ ) is computed as follows:

$$T = \frac{3}{2}p[\Psi_{PM}i_q + (L_d - L_q)i_d i_q], \quad (26)$$

where  $\Psi_{PM}$  is the linkage flux;  $L_d$  and  $L_q$  are respectively direct and quadrature axis inductances;  $i_d$  and  $i_q$  are respectively direct and quadrature axis currents. It should be noted that the torque in (26) can be defined via the Maxwell's stress force equation given in [26], i.e.,

$$T = \oint_s r \times \sigma \cdot dS \\ \oint r \times \left[ \frac{1}{\mu_0}(\mathbf{B} \cdot \mathbf{n})\mathbf{B} - \frac{1}{\mu_0}B^2 \cdot \mathbf{n} \right], \quad (27)$$

where  $\mathbf{n}$  is the unit normal,  $r$  is the coordinate system and  $\sigma$  is the stress tensor.

Finally, the magnetic vector potential formulation is presented via the expression as follows:

$$\nabla^2 \mathbf{A} + \sigma \mu \frac{d\mathbf{A}}{dt} = \mu_0 \nabla \times \mathbf{M}, \quad (28)$$

where  $\mathbf{M}$  is the magnetization vector and  $\nabla^2$  is the Laplacian.

## 5. Numerical Test

Based on the main dimensions of the proposed motors given in Table 2 obtained from the process of analytical model, in this part, the electromagnetic parameters of these motors are verified by the FEM to compare performances of six-phase SPMSMs with IR and OR types. The 2D geometry and mesh of the proposed SPMSMs are presented in Fig. 4 and Fig. 5, respectively.

The distribution waveforms of back electromotive force (EMF) and torque without using skewed PMs of the six-phase PMSM with IR and OR types are shown in Fig. 6 and Fig. 7, respectively. It can be seen that the waveforms for both cases of the back EMF and torque are still ripple and not sinusoidal. In order to overcome these drawbacks, the skewing technique is used to make sure that the back EMF waveform is sinusoidal as much as possible, which leads to the small value of torque ripple. One often used technique for reducing torque ripple and mitigating the cogging torque in PMSMs is rotor step skewing. As reference in [14], it not only modifies the stator's electromagnetic force distribution but also significantly affects the noise level that the motor emits.

Fig. 8 shows the PMs with skewing approach. The PMs must be segmented in order to use the skewing approach. The permanent magnet is initially split into 5

**Tab. 3:** Skew angles of the permanent magnet

| Slice   | Proportional length | Angle |
|---------|---------------------|-------|
| Slice 1 | 1                   | -6    |
| Slice 2 | 1                   | -3    |
| Slice 3 | 1                   | 0     |
| Slice 4 | 1                   | 3     |
| Slice 5 | 1                   | 6     |

portions for this investigation. Next, the skew angle is selected; for a symmetric instance, as indicated in Table 3, the permanent magnet skew angle is zero. These angles were selected at random to demonstrate the potential benefits of the skewing technique. Nonetheless, an optimization procedure can make use of these angles to get the greatest outcome with the least amount of torque ripple.

Fig. 9 has shown the results on a quarter view of distribution of magnetic flux density due to the symmetry of the motor. It can be seen that The maximum values of flux density are 2,08T and 2,11T for IR motor and OR motor respectively, which concentrate on tooth tips, where have small area when the magnetic flux passes through. These values are not too high so that the normal working operation of the motors will not suffer any problems. The simulation results are given in Table 4.

As we could see in Table 4, the output power and torque of the two motors satisfied the design requirements of 145kW and 1055Nm. The line-line back-EMF waveforms are given in Fig. 10 with the RMS values are 326,8V for IR motor and 366,7V for OR motor, respectively. All these values are still smaller than the terminal line voltage of 398,9V.

The output torque waveforms are shown in Fig. 11. The value of torque ripple of IR motor is 7,3% which is smaller than this value of OR motor of 8,4%. This is because the OR rotor has larger width of magnet and smaller width of tooth when compared to the IR motor, which will lead to more significant interaction force between magnet and stator tooth when each pole pass through stator teeth. This interaction will create larger cogging torque, which will result in more ripple on the waveform of output torque in OR motor in comparison with IR motor. The torque ripple waveforms of the two motors are presented in Fig. 12.

The efficiency of the two motors are almost the same with 95,12% of IR motor and 95,11% of OR motor. The output torque of OR motor is 1074,4 Nm, which is larger than the torque of 1068,5 Nm of IR motor due to slightly higher output power of OR motor in comparison with IR motor. The power factor of the two motors are also almost the same with the value of 0,92 and 0,91 of IR motor and OR motor respectively. Note that both IR and OR SPMSM are radial flux mo-

**Tab. 4:** Skew angles of the permanent magnet

| Parameter               | Inner Rotor | Outer Rotor | Unit               |
|-------------------------|-------------|-------------|--------------------|
| Output power            | 145,5       | 146,3       | kW                 |
| Total loss              | 7461,2      | 7524,2      | W                  |
| Efficiency              | 95,12       | 95,11       | %                  |
| Output torque           | 1068,5      | 1074,4      | Nm                 |
| Torque ripple           | 7,3         | 8,4         | %                  |
| Torque per rotor volume | 41,85       | 89          | kNm/m <sup>3</sup> |
| Power factor            | 0,92        | 0,91        |                    |
| THD Back-EMF            | 2,4         | 1,4         | %                  |

tors, so the radial flux density component in the air gap has significant amplitude when compared to the axial component and plays an essential role for electromagnetic transformation processes inside the motors. As we could see in Fig. 13, the radial air gap flux density of both IR and OR motor have significant harmonic amplitude as seen in Fig. 14. Normally, this result will lead to unexpected waveform of back EMF with large ripple as mentioned above in Fig. 6. However, thanks to the step rotor skewing technique, despite the bad waveform of flux density in the air gap, the back EMF waveforms of both motors are nearly sinusoidal with little harmonic amplitude as presented in Fig. 15. It can be seen that the better waveform of back EMF, the better output torque quality. As we could see in Fig. 11, the torque waveforms are much smoother with ripple value of IR motor of 7,3% when compared to that of 24,7% in Fig. 7.

The THD of back EMF of the two motors are low, which are 2,4% of IR motor and 1,4% of OR motor with the harmonic amplitude shown in Fig. 15. The flux linkage in no load and full load operation and their harmonic orders are also presented in Fig. 16 and Fig. 17.

The torque density, which is expressed as the ratio of torque to rotor volume or torque per rotor volume, is an important parameter of a motor as it defines the capability to carry torque of a motor in a given weight and space. From Table 4, we could see that the torque density of 89 kNm/m<sup>3</sup> of the OR motor is more than doubled that value of the IR motor, which is only 41,85 kNm/m<sup>3</sup>. This means that the OR motor is more suitable for low-speed applications as it provides better torque-carrying capability when compared to the IR motor.

## 6. Conclusion

In this paper, the analytical and numerical methods have been successfully proposed to calculate and simulate a 145kW six-phase SPMSM with IR and OR configurations. The step rotor skewing technique has been also employed in order to reduce torque ripples. The simulation results show that the two SPMSMs archive the requirements of the design parameters. The results on the efficiency, output torque, cogging torque, torque ripple, torque density, harmonic components of back EMF, air gap flux density, flux linkage under no load and full load operations of the two these machines are then compared to each other. It can be observed that the SPMSM with IR structure has less torque ripple on the output torque waveform in comparison with the SPMSM with OR type, which means that the SPMSM with IR prototype has better torque quality than that of the SPMSM with OR configuration. However, the much larger torque density value of the OR type makes it more suitable for high-torque applications when compared to the that of IR type. The design optimization for these motors to archive the optimal results in efficiency, torque ripple and material cost will be developed in next studies.

## Acknowledgment

This research is funded by Hanoi University of Science and Technology under project number T2023-PC-043.

## Author Contributions

V.D.Q developed the proposed the analytical model and finite element method for the SPMSM with IR and OR configurations. T.T.C applied the FEM to simulate the electromagnetic parameters of the proposed machine. T.N.V checked and analysed results. H.V.T re-checked all the contents of the manuscript. All authors contributed to the final version of the manuscript

## References

- [1] H. Won, Y. -K. Hong, J. Platt, M. Choi, B. Bryant and S. Choi. Six-phase Fractional-slot Concentrated Winding Ferrite Spoke-type Permanent Magnet Synchronous Motor for Electric Truck. *2021 IEEE International Electric Machines & Drives Conference (IEMDC)*, Hartford, CT, USA. 2021, pp. 1-6. ISBN 978-1-6654-0510-2. DOI: 10.1109/IEMDC47953.2021.9449491.

- [2] F. Jin, J. Si, Z. Cheng, P. Su, L. Dong and G. Qi. Analysis of a Six-Phase Direct-Drive Permanent Magnet Synchronous Motor with Novel Toroidal Windings. *2019 IEEE Vehicle Power and Propulsion Conference (VPPC)*, Hanoi, Vietnam. 2019, pp. 1-6. ISBN 978-1-7281-1250-3. DOI: 10.1109/VPPC46532.2019.8952311.
- [3] M. Z. Islam, S. S. R. Bonthu and S. Choi. Comparison of two different winding topologies for external-rotor five-phase PM-assisted synchronous reluctance motor in vehicle applications. *2017 IEEE International Electric Machines and Drives Conference (IEMDC)*, Miami, FL, USA. 2017, pp. 1-6. ISBN 978-1-5090-4282-1. DOI: 10.1109/IEMDC.2017.8002399.
- [4] Sculler, F. & Semail, Eric & Charpentier, Jean-Frederic & Letellier, Paul. (2009). Multi-criteria-based design approach of multi-phase permanent magnet low-speed synchronous machines. *Electric Power Applications. IET*. 2009, vol. 2, iss. 2, pp. 102-110. ISSN 1751-8679. DOI: 10.1049/iet-epa:20080003.
- [5] V. I. Patel, J. Wang, W. Wang and X. Chen. Six-Phase Fractional-Slot-per-Pole-per-Phase Permanent-Magnet Machines With Low Space Harmonics for Electric Vehicle Application. *IEEE Transactions on Industry Applications*. 2014, vol. 50, no. 4, pp. 2554-2563. ISSN 1939-9367. DOI: 10.1109/TIA.2014.2301871.
- [6] Yanqi, Wei & Si, Ji & Cheng, Zhiping & Xu, Shuai & Dong, Lianghui & Liang, Jing. (2021). Design and characteristic analysis of a six-phase direct-drive permanent magnet synchronous motor with 60° phase-belt toroidal winding configuration for electric vehicle. *IET Electric Power Applications*. 2021, vol.14, iss. 13, pp. 2659-2666. ISSN 1751-8679. DOI: 10.1049/iet-epa.2020.0083
- [7] L. Cheng, Y. Sui, P. Zheng, Z. Yin and C. Wang. Influence of Stator MMF Harmonics on the Utilization of Reluctance Torque in Six-phase PMA SynRM with FSCW. *Energies*. 2017, vol. 11, iss. 108, pp. 1-17. ISSN 1996-1073. DOI: 10.3390/en11010108
- [8] L. V. Iyer, C. Lai, H. Dhulipati, S. Mukundan, K. Mukherjee and N. Kar. Investigation of a Six-Phase Interior Permanent Magnet Synchronous Machine for Integrated Charging and Propulsion in EVs. *SAE international journal of alternative powertrains*. 2018, vol. 7, no. 2, pp. 14. ISSN 2167-4191. DOI: 10.4271/08-07-02-0006.
- [9] Li, Xianglin, Yingjie Tan, Bo Yan, Yujian Zhao, and Hao Wang. 2023. Demagnetization Modeling and Analysis for a Six-Phase Surface-Mounted Field-Modulated Permanent-Magnet Machine Based on Equivalent Magnetic Network. *Energies*. 2023, vol. 16, iss. 16, pp. 1-19. ISSN 1996-1073. DOI: h10.3390/en16166099.
- [10] A. M. El-Refaie, J. P. Alexander, S. Galioto, P. B. Reddy, K. Huh, P. Bock, and X. Shen. Advanced high power-density interior permanent magnet motor for traction applications. *2013 IEEE Energy Conversion Congress and Exposition*, Denver, CO, USA, 2013, pp. 581-590. ISBN 978-1-4799-0336-8. DOI: 10.1109/ECCE.2013.6646754
- [11] H. Won, Y. Hong, W. Lee, and M. Choi. Roles of coercivity and remanent flux density of permanent magnet in interior permanent magnet synchronous motor (IPMSM) performance for electric vehicle applications. *AIP Advances*. 2018, 8, pp. 056811. DOI: 10.1063/1.5007789.
- [12] F. Jin, J. Si, Z. Cheng, P. Su, L. Dong and G. Qi. Analysis of a Six-Phase Direct-Drive Permanent Magnet Synchronous Motor with Novel Toroidal Windings. *2019 IEEE Vehicle Power and Propulsion Conference (VPPC)*, Hanoi, Vietnam. 2019, pp. 1-6. ISBN 978-1-7281-1249-7. DOI: 10.1109/VPPC46532.2019.8952311.
- [13] H. M. Taha and I. Alnaab. Designs of PMSMs with Inner and Outer Rotors for Electric Bicycle Applications. *KJAR*. 2019, vol. 4, no. 1, pp. 20–25. ISSN 2411-7706. DOI: 10.24017/science.2019.1.4.
- [14] Gao, Caixia, Mengzhen Gao, Jikai Si, Yihua Hu, and Chun Gan. A Novel Direct-Drive Permanent Magnet Synchronous Motor with Toroidal Windings. *Energies*. 2019, vol. 12, iss. 3, pp. 1-14. ISSN 1996-1073. DOI: 10.3390/en12030432.
- [15] G. Heins, D. Ionel and M. Thiele. Winding factors and magnetic fields in permanent magnet brushless machines with concentrated windings and modular stator cores. *2013 IEEE Energy Conversion Congress and Exposition*, Denver, CO, USA. 2013, pp. 5048-5055. DOI: 10.1109/ECCE.2013.6647382.
- [16] J. H. J. Potgieter and M. J. Kamper. Double PM-Rotor, Toothed, Toroidal-Winding Wind Generator: A Comparison With Conventional Winding Direct-Drive PM Wind Generators Over a Wide Power Range. *IEEE Transactions on Industry Applications*. 2016, vol. 52, iss. 4, pp. 2881-2891. ISSN 1939-9367. DOI: 10.1109/TIA.2016.2536580.
- [17] R. Madhavan and B. G. Fernandes, "Axial Flux Segmented SRM With a Higher Number of Rotor Segments for Electric Vehicles. *IEEE Transactions on Energy Conversion*. 2013, vol. 28, no. 1, pp. 203-213. ISSN 1939-9367. DOI: 10.1109/TEC.2012.2235068.

- [18] Z. Q. Zhu and D. Howe. Influence of design parameters on cogging torque in permanent magnet machines. *IEEE Transactions on Energy Conversion*. 2020, vol. 15, no. 4, pp. 407-412. ISSN 1558-0059. DOI: 10.1109/60.900501.
- [19] L. Zhu, S. Z. Jiang, Z. Q. Zhu and C. C. Chan. Analytical Methods for Minimizing Cogging Torque in Permanent-Magnet Machines. *IEEE Transactions on Magnetics*. 2009, vol. 45, no. 4, pp. 2023-2031. ISSN 1941-0069. DOI: 10.1109/TMAG.2008.2011363.
- [20] Won, Hoyun, Yang-Ki Hong, Minyeong Choi, Jonathan Platt, Briana Bryant, Seungdeog Choi, Shuhui Li, Hwan-Sik Yoon, Timothy A. Haskew, Jongkook Lee, and et al. 2022. Novel Design of Six-Phase Spoke-Type Ferrite Permanent Magnet Motor for Electric Truck Application. *Energies*. 1997, vol. 15, iss. 6. ISSN 1996-1073. DOI: 10.3390/en15061997.
- [21] L. I. Jusoh, E. Sulaiman, F. S. Bahrim and R. Kumar. Design Comparison of Inner and Outer Rotor of Permanent Magnet Flux Switching Machine for Electric Bicycle Application. *2017 IOP Conf. Ser.: Mater. Sci. Eng.* 226 012129. DOI: 10.1088/1757-899X/226/1/012129.
- [22] H. M. Taha and I. R. Alnaab. Designs of PMSMs with Inner and Outer Rotors for Electric Bicycle Applications. *Kurdistan Journal of Applied Research*. 2019, vol. 4, iss. 1, pp. 20-25. ISSN 2411-7706. DOI: 10.24017/science.2019.1.4.
- [23] V. X. Hung, "Modeling of exterior rotor permanent magnet machines with concentrated winding," *Doctoral Thesis*, Technische Universiteit Delft, 2012.
- [24] T. Jokinen, V. Hrabovcova and J. Pyrhonen. Design of Rotating Electrical Machines. *John Wiley & Sons Ltd*, 2008.
- [25] H. Liu. Design of High-Efficiency Rare-Earth Permanent Magnet Synchronous Motor and Drive System. *Electronic Thesis and Dissertations*, STARS, 2015.
- [26] Naik, Supriya & Bag, Baidyanath & Chandrasekaran, Kandasamy. (2021). Comparative Analysis of Surface Mounted and Interior Permanent Magnet Synchronous Motor for Low rating Power Application. *Journal of Physics: Conference Series*. 2070. 012119. 10.1088/1742-6596/2070/1/012119.

## About Authors

**Vuong Dang QUOC** received his PhD degree in 2013 from the Faculty of Applied Sciences at the University of Liège in Belgium. After that he came back to the Hanoi University of Science and Technology in September 2013, where he is currently working as a deputy director of Training Center of Electrical Engineering, School of Electrical Engineering, Hanoi, University of Science and Technology. He became an associate professor in 2020. Assoc. Prof. Dang Quoc Vuong's research domain encompasses modeling of electromagnetic systems, electrical machines, optimization method, numerical methods and subproblem methods. He can be contacted at email: [vuong.dangquoc@hust.edu.vn](mailto:vuong.dangquoc@hust.edu.vn).

**Trinh Cong TRUONG** (corresponding author) received the Engineer degree in 2021 from the Department of Electrical Engineering, School of Electrical Engineering, Hanoi University of Science and Technology. He is currently working as a master student at the Department of Electrical Engineering, Hanoi University of Science and Technology. He can be contacted at email: [trinh.congtruong@hust.edu.vn](mailto:trinh.congtruong@hust.edu.vn).

**Thanh Nguyen VU** received his PhD degree in 2015 from the Department of Electrical Engineering, School of Electrical Engineering, Hanoi University of Science and Technology. He is currently working as a head of Laboratory of High performance electric machines (HiPems). He can be contacted at email: [thanh.nguyenvu@hust.edu.vn](mailto:thanh.nguyenvu@hust.edu.vn).

**Ha Vo THANH** received a Ph.D. degree from the Hanoi University of Science and Technology, Viet Nam, in 2020, both in Control and Automation Engineering. Her research interests include the field of electrical drive systems, power electronics, and electric vehicles. She can be contacted at email: [vothanhhha.ktd@utc.edu.vn](mailto:vothanhhha.ktd@utc.edu.vn).

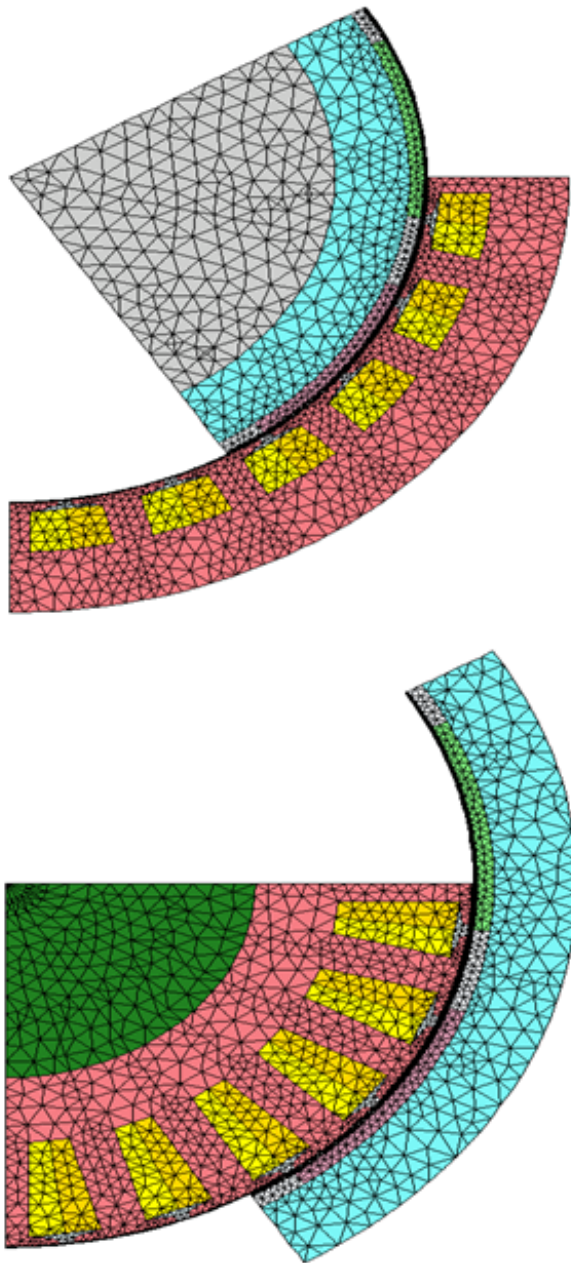


Fig. 5: D-Mesh of the SPMSM: Inner rotor (top) and outer rotor (bottom).

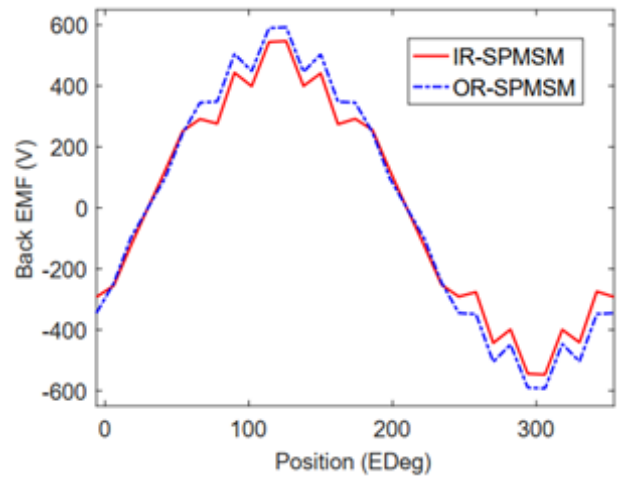


Fig. 6: Back EMF waveform without using the skewing technique with IR and OR.

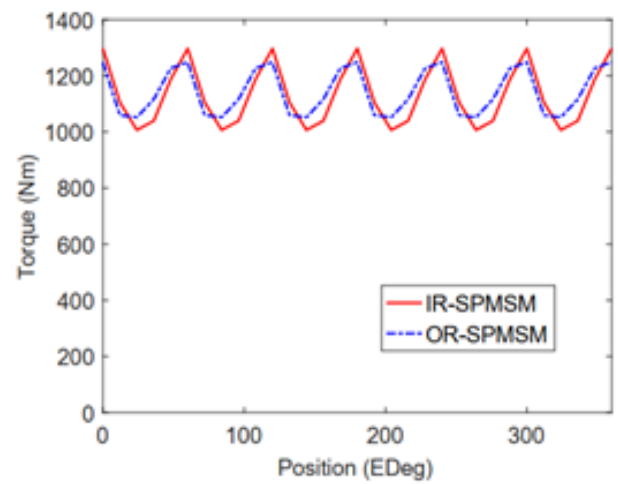


Fig. 7: Back EMF waveform without using the skewing technique with IR and OR.

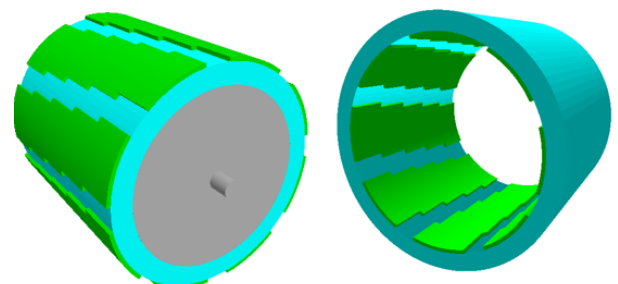


Fig. 8: PMs with skewing technique with IR and OR.

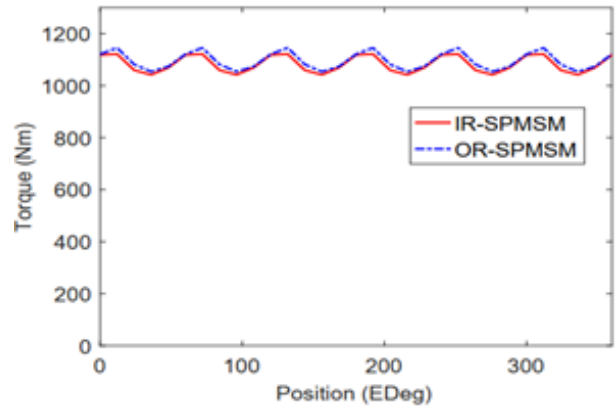
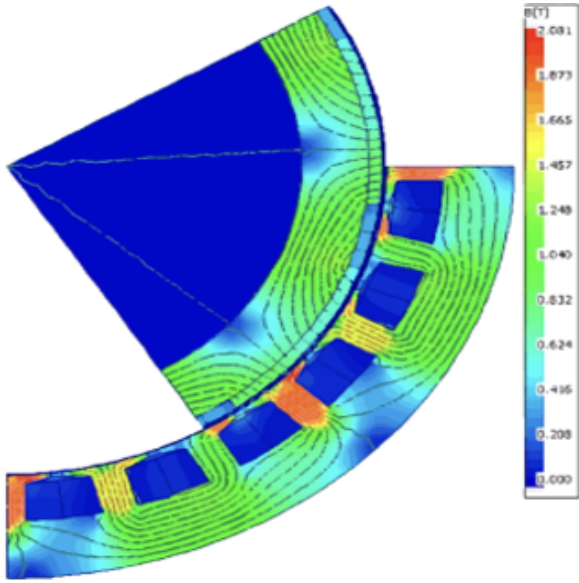


Fig. 11: Output torque waveforms of SPMSM with inner rotor (IR) and outer rotor (OR).

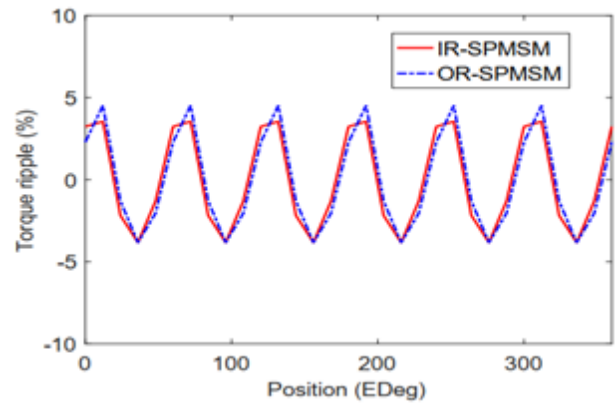
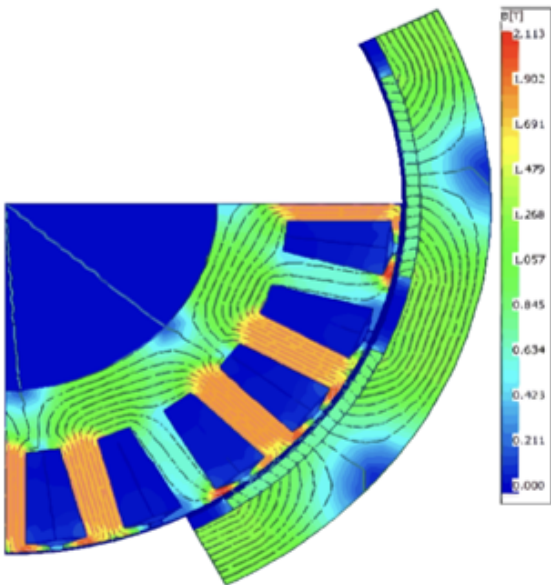


Fig. 12: Torque ripple waveforms of SPMSM with IR and OR.

Fig. 9: Flux density distribution with IR and OR.

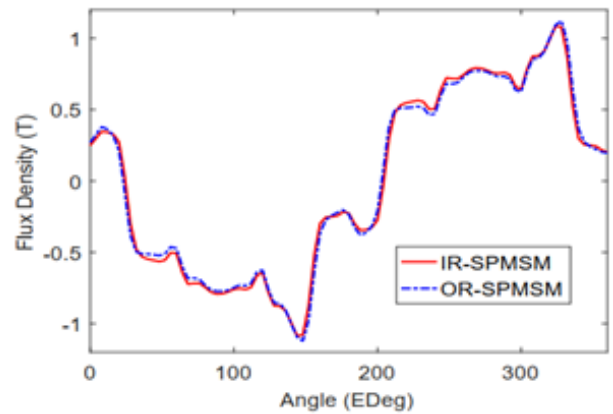
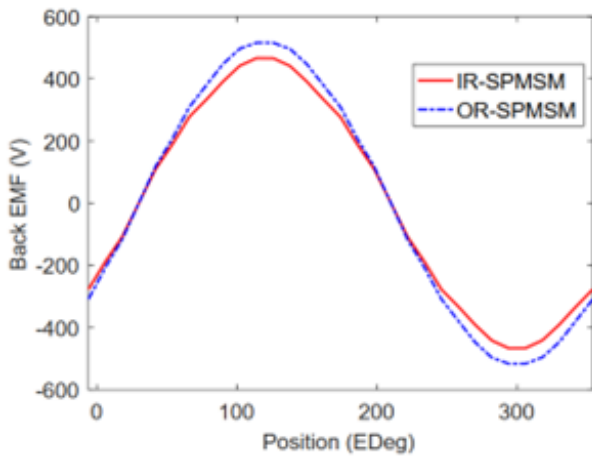


Fig. 13: Flux density waveforms of SPMSM with IR and OR.

Fig. 10: Back EMF waveforms of SPMSM with IR and OR.

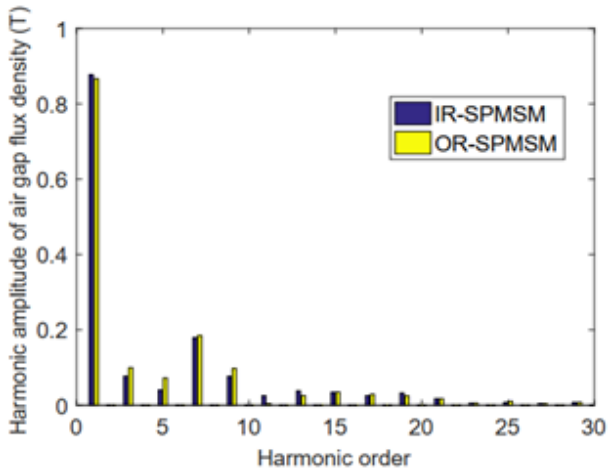


Fig. 14: The harmonic amplitudes of air gap flux density with IR and OR.

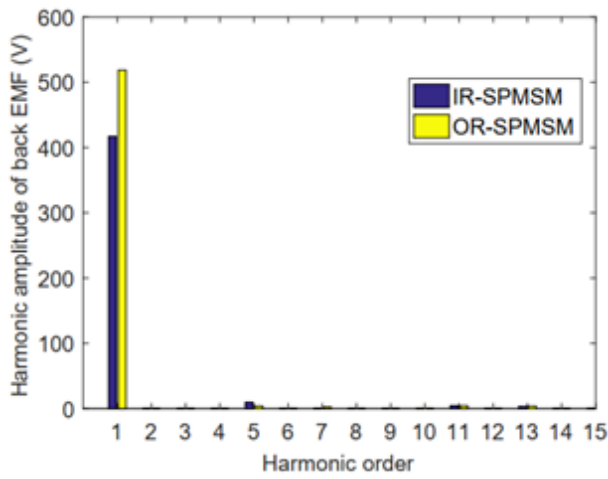


Fig. 15: Harmonic amplitude of back EMF with IR and OR.

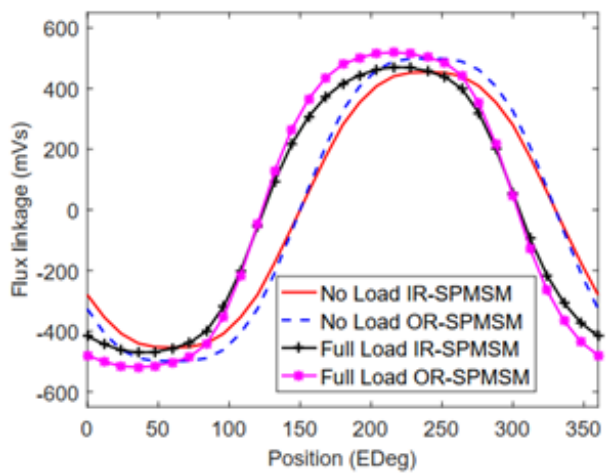


Fig. 16: Flux linkage in no load and full load operation with IR and OR.

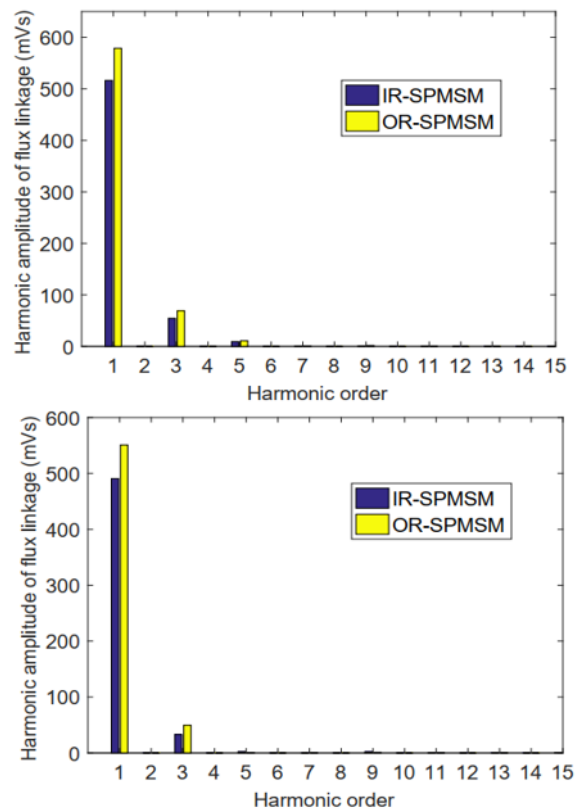


Fig. 17: Harmonic components of flux linkage with IR and OR under no load (top) and full load (bottom).